The effect of indenter shape on sub-micron indentation according to discrete dislocation plasticity

Widjaja, A.; Needleman, A.; Van der Giessen, E.

The effect of indenter shape on sub-micron indentation according to discrete dislocation plasticity

A Widjaja[1], A Needleman[2] and E Van der Giessen[1]

[1] Materials Science Centre, University of Groningen, Nyenborgh 4, 9747 AG Groningen,
The Netherlands
[2] Division of Engineering, Brown University, Providence, RI 02912, USA

Abstract
Two-dimensional discrete dislocation simulations of indentation in the sub-micron range are presented for wedge indenters with a sharp tip and for indenters with a circular tip. Plane strain calculations are carried out for single crystals that are initially free of mobile dislocations and with all dislocations nucleating from a specified distribution of internal sources. The hardness is expressed in terms of the indentation force divided by the actual contact area accounting for roughness of the surface in contact with the indenter. For wedge indenters the hardness is found to decrease with increasing indentation depth, while for indenters with a circular tip the hardness increases somewhat with increasing indentation depth. However, at a given indentation depth, the indentation hardness of circular indenters increases with decreasing tip radius. The difference in hardness evolution for the two tip shapes is mainly due to the manner in which the evolution of the contact area depends on indenter tip shape. The nominal hardness, i.e. that based on the geometric contact area neglecting material sink-in or pile-up and surface roughness, is found to follow the inverse square root size dependence predicted by Nix and Gao [1] and by Swadener *et al* [2], even though the plastic zone found in the simulations differs significantly in shape and size from that assumed in deriving the scaling laws.

1. Introduction

Submicron scale indentation hardness of crystalline solids exhibits a distinct size effect, with smaller generally being harder. This indentation size effect has been rationalized in terms of the presence of geometrically necessary dislocations associated with the plastic strain gradients in the vicinity of the indenter, [1]. Ideally, for a perfectly sharp wedge or conical indenter, the hardness is independent of the indentation depth (or, equivalently, contact area) if the material response is scale independent. The existence of the indentation size effect is one of the key pieces of evidence for a plastic material length scale in the submicron range. However, in an indentation experiment the conditions for the ideal scale-independent response are never actually realized. At micron-scale indentation depths, length scales associated with surface

Figure 1. Schematic of the indentation of a symmetric crystal of $2L_1 \times L_2$ by (*a*) a wedge indenter characterized by wedge semi-angle α or (*b*) a circular indenter of radius R. Plasticity by the motion of edge dislocations is allowed in a process window of $l_1 \times l_2$ that is confined within a significantly larger, perfectly adhering crystal with three slip systems.

oxide layers or surface roughness could possibly come into play. Also, indenters are never ideally sharp and self-similar so that a length scale (or scales) associated with the indenter can affect the inferred hardness. Indeed, significant effects of indenter shape are observed experimentally, e.g. [2–4]. Also, such effects are seen in indentation calculations using a phenomenological size-dependent plastic flow rule [5].

Here, we employ discrete dislocation plasticity to study the effects of indenter shape on hardness. Plane strain analyses are carried out for single crystals indented by wedge or circular indenters. Plastic flow arises from the glide of dislocations generated by Frank–Read sources in the bulk. For the wedge indenter the key length scale is the material length scale, while for the circular indenter there is a complex interaction between the material length scale and the indenter radius, as seen in the simulations in [6]. Results are presented for the variation of the indentation size effect with indenter shape. The effect of dislocation source density is also briefly explored.

2. Problem definition

We study a two-dimensional crystal, of size $2L_1 = 200\,\mu\text{m}$ by $L_2 = 200\,\mu\text{m}$, which is indented on the face $x_2 = 0$ and fixed to a rigid substrate at the opposite side $x_2 = L_2$, figure 1(*a*). The lateral sides $x_1 = \pm L_1$ are traction free and plane strain conditions are imposed perpendicular to the x_1–x_2-plane of view. The crystal is assumed to be symmetric about the plane $x_1 = 0$ so that only half of the crystal, $x_1 \geqslant 0$, is modelled.

The crystal is indented in the x_2-direction with the indenter making first contact with the crystal at $(0, 0)$ as sketched in figure 1. Two indenter tip shapes are considered: (i) wedge indenters with a tip semi-angle α and (ii) circular indenters of radius R, figure 1.

Plastic deformation of the crystal takes place by the motion of edge dislocations on three slip systems, which are oriented at angles $\phi^{(\beta)}$ ($\beta = 1, 2, 3$) of $\{35.3°,\ 90.0°,\ 144.7°\}$ relative to the surface $x_2 = 0$, as illustrated in figure 1(*b*). This orientation allows for the double slip necessary for the assumed symmetry.

The elastic properties of the crystal are taken to be isotropic and have values typical for aluminium; shear modulus $G = 26\,\text{GPa}$ and Poisson's ratio of $\nu = 0.33$. In a discrete dislocation plasticity framework, the dislocations are treated individually, as singularities in an

otherwise linear elastic continuum, and the magnitude of the Burgers vector of all dislocations is $b = 0.25$ nm. Slip planes within each of the three slip systems are spaced at $100b$ inside a square process window with side length $2l_1 = l_2 = 50 \, \mu$m centered around the indenter tip (figure 1). The process window is introduced for numerical convenience and does not affect the results; the computations are terminated before any dislocation reaches the process window boundary. Initially, the crystal is stress and dislocation free, but contains a random distribution of dislocation sources with density ρ_{nuc} and of dislocation obstacles with density ρ_{obs}. The sources are two-dimensional versions of Frank–Read sources, which generate a dipole of edge dislocations when the resolved shear stress on the source is large enough ($\geqslant \tau_{nuc}$) for a sufficiently long time t_{nuc}. The obstacles pin a dislocation when it attempts to pass by; pinned dislocations are released when the Peach–Koehler force exceeds the obstacle strength $b\tau_{obs}$. Dislocation glide is taken to be drag controlled, with the dislocation velocity proportional to the magnitude of the Peach–Koehler force and the drag coefficient being $10^4 \, (\text{Pas})^{-1}$. When dislocations of opposite sign come within $6b$ they annihilate.

Even though we perform a small-strain analysis, the boundary conditions evolve with indentation depth because of the continuously changing region over which contact takes place. Denoting the current contact surface by S_c, continued indentation is prescribed through the displacement-rate conditions

$$\dot{u}_1 = 0, \ \dot{u}_2 = \dot{h} \text{ on } S_c, \tag{1}$$

assuming that the material sticks to the indenter when it moves with a velocity $\dot{h}$ in the x_2-direction. The other boundary conditions are

$$\dot{u}_1 = 0, \ \dot{T}_2 = 0 \text{ on } x_1 = 0, \tag{2}$$

because of symmetry, and

$$\dot{T}_1 = \dot{T}_2 = 0 \text{ on } x_2 = 0 \notin S_c. \tag{3}$$

Here, $T_i = \sigma_{ij}n_j$ is the traction on the surface with normal n_j directing outward from the surface. Recalling the symmetry of the problem, the half-indentation force F is calculated as

$$F = -\int_{S_c} T_2 \, \mathrm{d}x_1.$$

The problem is solved in an incremental manner, making use of the superposition method of Van der Giessen and Needleman [7] to incorporate the boundary conditions (1)–(3). This framework has been used to analyse a variety of boundary value problems, giving predictions that are qualitatively, e.g. [8–11], and quantitatively, [12], in accord with experiment and that provide insight into the origin of, for example, the observed size effects. The finite element mesh used in this study is highly refined near the indenter tip to accurately represent contact.

Figure 2 not only shows an example of the mesh used, but also illustrates that the initially flat surface of the crystal roughens as dislocations exit the crystal through the free surface. As a consequence, contact builds up in the form of patches with a compressive traction between crystal and indenter. The sum of these patches forms the true contact area or contact length in two dimensions, a, which thus specifies S_c. In [13], we have compared the use of this definition of contact area for wedge indenters (denoted there by a_A) with other definitions, such as nominal contact length a_N or that proposed by Oliver and Pharr [14]. It was found that the other definitions tend to overestimate the contact area, and thus underestimate hardness, with the difference being larger for sharper indenters. In this paper, unless stated otherwise, the hardness is defined using the actual contact length a sketched in figure 2.
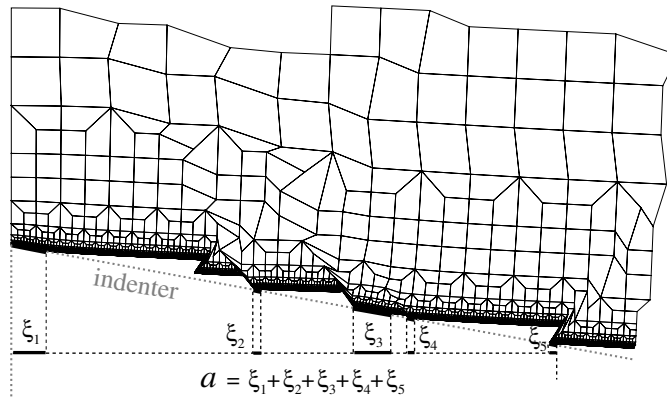
Figure 2. Illustration of the determination of the actual contact length a for a rough surface. The finite element mesh is typical for the computations reported here.

3. Numerical results

In a discrete dislocation plasticity analysis, the initial dislocation structure needs to be specified. In the framework here, this initial dislocation structure is represented by a random distribution of dislocation sources and obstacles with given densities. Most results presented are for crystals with a source density $\rho_{nuc} = 49\,\mu m^{-2}$ and an obstacle density $\rho_{obs} = 99\,\mu m^{-2}$. Crystals with these densities are referred to as high source density (HSD) crystals since subsequently we show the effect of a significantly lower source density (LSD): $\rho_{nuc} = 9\,\mu m^{-2}$ and $\rho_{obs} = 18\,\mu m^{-2}$. The strength of the sources τ_{nuc} follows a Gaussian distribution with mean value of 50 MPa and standard deviation of 10 MPa. The nucleation time is $t_{nuc} = 10$ ns in all calculations. The obstacle strength τ_{obs} is 150 MPa. Uniaxial tension (or compression) simulations of specimens having the size of the process window, $2l_1 = l_2 = 50\,\mu m$ by $2l_1 = l_2 = 50\,\mu m$, (see figure 1(*a*)) give an overall yield strength of about 50 MPa for the HSD crystals and 60 MPa for the LSD crystals.

Calculations are carried out for wedge indenters with $\alpha = 70°$ and $\alpha = 85°$ and for circular indenters with radii of $R = 0.25, 0.5, 1, 2$ and $4\,\mu m$. For wedge indentation, we report the average of three realizations of source and obstacle distributions, while for circular indentation the results are for one realization. The finite element mesh is highly refined near the indenter tip, with the smallest element length near the tip being 0.24 nm for the wedge indenters and 1 nm for the circular indenters.

The evolution of (half) the indentation force F with increasing indentation depth h is shown in figure 3(*a*) for the circular indenters. For comparison purposes, results for $\alpha = 70°$ wedge indentation are also shown. Initially, the slope is high and almost independent of indenter shape. However, when plastic flow by the collective motion of dislocations initiates, dF/dh decreases but less so for large circular indenters than for small circular indenters or for wedge indenters. While the force on the $\alpha = 70°$ wedge indenter tends to increase linearly with depth after about $h = 0.2\,\mu m$, the force on the circular indenters increases less than proportionally with depth. The raggedness of the curves is mainly due to individual nucleation events and is sensitive to statistical fluctuations; the results for wedge indentation are smoother than for circular indentation because they are averaged over three realizations.

As indentation progresses, the contact length increases. The evolution of contact length a versus depth h is shown in figure 3(*b*). For the relatively sharp wedge indenter with $\alpha = 70°$, the contact length is small because of sink-in. The large error bar around $h = 0.4\,\mu m$ is caused
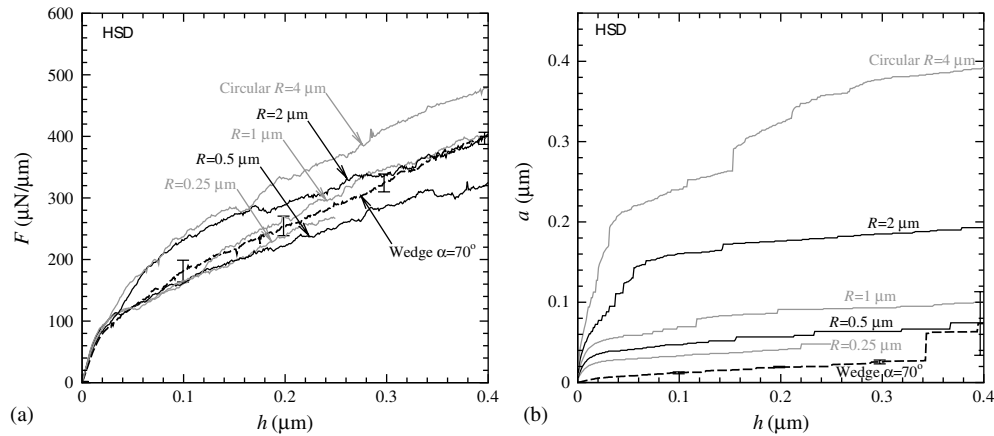
**Figure 3.** Evolution of (*a*) the indentation half-force *F* and (*b*) the contact length *a* with indentation depth for 70°-wedge and circular indenters with various radii. The wedge results are averaged over three realizations and the error bars give an impression of the spread.

by jumps in contact length in some of the three realizations. These jumps occur for two reasons. First, due to material sink-in a portion of the deformed material surface outside the contact tends to become almost parallel to the indenter surface so that when indentation continues and the indenter touches the surface of the crystal, the contact length suddenly increases. Secondly the surface roughens and, as discussed in detail by Widjaja *et al* [13], this also leads to abrupt increases in contact length. The predicted increase in the contact length *a* for the circular indenters in figure 3(*b*) exhibits the same general trend, with occasional jumps in contact length occurring with the average d*a*/d*h* decreasing for increasing indentation depth. Also, the contact length increases with increasing indenter radius. For a given indentation depth, the contact length is a strong function of indenter shape, but the contact force is much less sensitive to indenter shape.

Figure 4 shows distributions of dislocations and normal stress in the direction of indentation, σ_{22}, for an $\alpha = 70°$ wedge indenter and a circular indenter with $R = 2\,\mu$m. The nominal contact lengths noted in figure 4 are quite different for these two indenters. However, the overall dislocation and stress distributions are quite similar. It is noted that in both cases the dislocation distribution extends over a distance of several micrometres, which is much larger than the indentation depth, the contact length (see figure 3) or the nominal contact length. Since all dislocations have nucleated inside the envelope of the dislocation distribution, Figure 4 gives an indication of the region in which dislocations have moved and produced plastic deformation.

3.1. Hardness

The hardness $H := F/a$ is shown as a function of depth *h* in figure 5. For $\alpha = 70°$ wedge indentation, the hardness decreases with increasing depth, revealing the usual indentation size effect. The drop in hardness around $h = 0.34\,\mu$m and $h = 0.4\,\mu$m is caused by the jumps in contact length; the large error bar around $h = 0.4\,\mu$m corresponds to the error bar in contact length (figure 3(*b*)). The hardness is high since the contact length is small. For comparison, in figure 5 we also include the hardness for $\alpha = 85°$ wedge indentation, which is lower than the hardness for $\alpha = 70°$ as the contact length is significantly larger [13]. For the larger tip
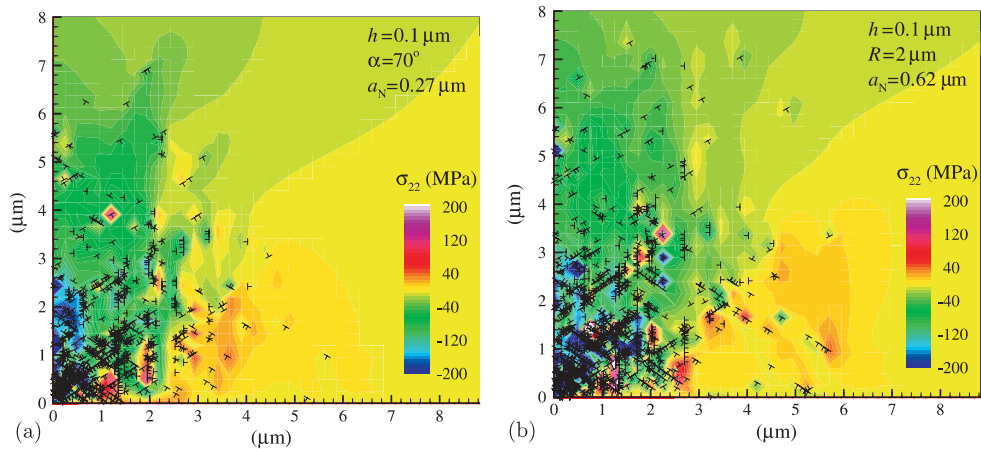
Figure 4. Dislocation distributions and contours of σ_{22} in HSD crystals when indented to $h = 0.1\,\mu\text{m}$ by (*a*) an $\alpha = 70°$ wedge or (*b*) an $R = 2\,\mu\text{m}$ circular indenter.
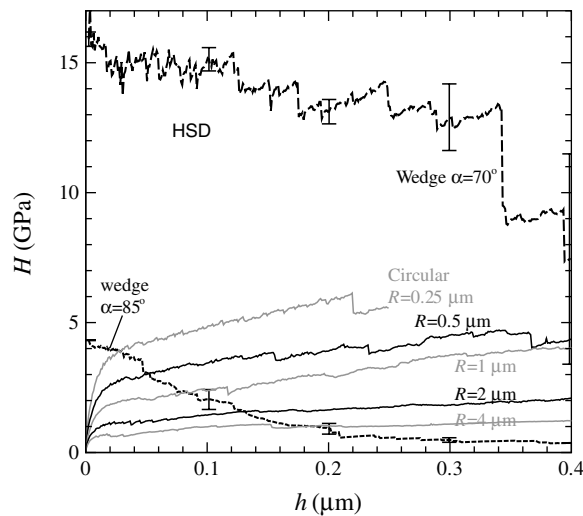
Figure 5. Hardness $H = F/a$ as a function of indentation depth h for wedge and circular indenters. The results for wedge indenters with $\alpha = 70°$ and $85°$ are averaged over three realizations and the error bars illustrate the spread among the individual simulations.

angle, the hardness clearly shows the typical size effect for wedge indentation, levelling off at a constant value of around $H = 0.4\,\text{GPa}$ at $h = 0.4\,\mu\text{m}$. This levelling off is not yet visible for $\alpha = 70°$. Over the range of indentation depths studied, the hardness found with $70°$ indenters is several times higher than that for the more shallow $85°$ indenters, which is still almost an order of magnitude higher than the yield stress of $50\,\text{MPa}$. The sensitivity to indenter tip angle is already present in the elastic regime; in fact, when sink-in is neglected, the elastic H scales with $\cot\alpha$ [15].

On the other hand, for circular indentation, the hardness increases with depth. The initial rapid increase of hardness with indentation depth occurs while the deformations are mainly elastic. At larger indentation depths, and for indenters with larger indenter radii, the
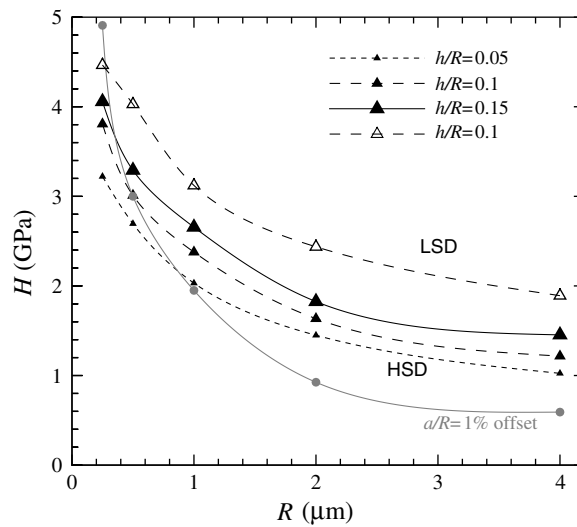
Figure 6. Dependence of hardness on the radius of circular indenters for fixed values of h/R and for values of a/R that correspond to a 1% elastic offset in the $H-a/R$ curves of figure 7. The curves through the data points serve merely as a guide to the eye.

hardness becomes less sensitive to depth. Thus, for circular indenters, once significant plastic deformation has occurred, the hardness does not increase much with indentation depth. At a given indentation depth, on the other hand, the hardness increases with decreasing indenter radius (as summarized in figure 6). In this sense, 'smaller is harder' for indentation with a circular indenter.

Another way to present the circular indenter results is by plotting hardness versus relative contact size a/R (see figure 7). By analogy with spherical indenters [16], a/R can be interpreted as a strain measure (up to a scaling factor). When one additionally invokes the Tabor relation between hardness and flow strength, $H \approx 3\sigma_f$, the curves in figure 7 can be regarded as effective stress–strain curves. For each value of R, the curves show strain hardening of the crystal. With strain being defined as $0.2a/R$ [16, 2] one can determine the 0.2% 'yield' point by the intersection of each of the $H-a/R$ curves with a line parallel to the elastic part that intersects $a/R = 0.01$. The hardness values thus found, shown in figure 6 by the gray dots, exhibit a 'smaller is harder' size effect; one that is even stronger than that for fixed h/R. The lowest yield strength of $0.7/3 = 0.23$ GPa for the largest indenter radius $R = 4\,\mu$m is substantially larger than the uniaxial compression yield strength 50 MPa but is lower than what is obtained with sharp indenters at the same penetration depth.

3.2. Effect of source density

The densities of dislocation sources and obstacles can vary significantly due, for example, to differences in prior plastic deformation. To explore the dependence of the indentation hardness on the source and obstacle densities, some of the calculations have been repeated for LSD crystals which have an approximately five times lower source and obstacle densities ($\rho_{nuc} = 9\,\mu$m^{-2} and $\rho_{obs} = 18\,\mu$m^{-2}). We recall that the uniaxial response of the LSD crystals equal to the process window is essentially the same as that of the HSD crystals.

The indentation response, presented in figure 8, does however change significantly. Since fewer sources are activated in the LSD crystals near the indenter, the indentation forces for all
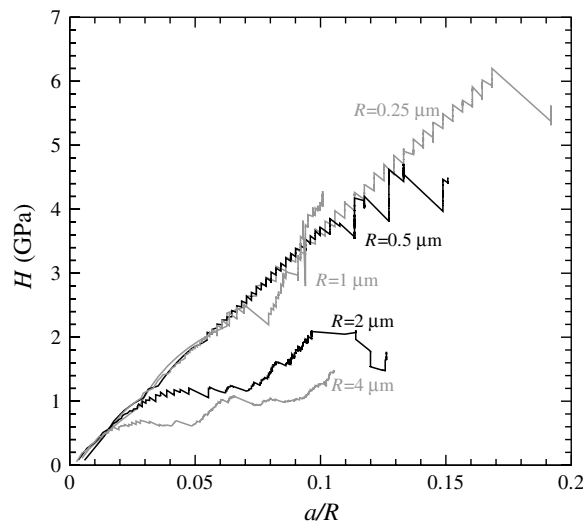
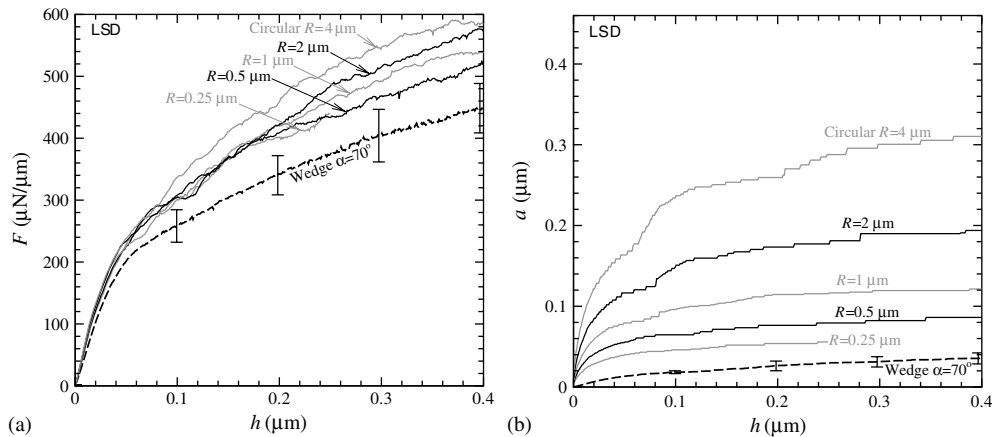**Figure 7.** Variation of hardness with a/R for various indenter radii R.

Figure 8. Evolution of (*a*) indentation force and (*b*) contact length with indentation depth for a crystal with a low density of sources and obstacles. The wedge results are averaged over three realizations and the error bars give an impression of the spread.

indenters are higher than in the corresponding HSD material (figure 3(*a*)). Quite interestingly, while the scatter in the 70° wedge results has increased, the effect of the reduced source and obstacle density seems to be smaller than for the circular indenters. However, for the circular indenters the contact length is rather insensitive to source density, at least for radii $R \leqslant 2\,\mu$m, figure 8(*b*) versus figure 3(*b*). As a consequence, the hardness of the LSD crystals is higher than that in figure 5 for the HSD crystals.

4. Discussion

The notion of an indentation size effect, with smaller being harder, depends on the measure of size used. In the case of a wedge indenter, which is self-similar, the only relevant geometrical

length scale in the problem is h. As seen in figure 5, the hardness versus indentation depth, $H(h)$, is a decreasing function. For circular indenters, there are two length scales, h and R, so that the hardness versus size function is of the form $H(R; h/R)$ or $H(h; h/R)$. However, since the hardness for circular indenters does not vary much with h except at very small h when plasticity has not initiated (see figure 5), the size effect then emerges through the dependence on indenter radius R and figure 6 shows that in this sense 'smaller is harder' for any value of h/R.

The wedge and circular indenters considered are, respectively, the two-dimensional equivalents of Vickers or Berkovich and spherical indenters used in experiments. The indentation size effect for our wedge indenters, with H decreasing with increasing h, is consistent with experimental nano- and micro-hardness results using sharp indenters, e.g. [17, 2, 4].

The hardness values reported are based on using the actual contact length a (see figure 2), taking into account the roughening of the surface due to slip steps left after dislocations have left the crystal. Another, simpler definition of contact is the nominal contact length a_N which is determined by the intersection of the indenter at a given depth with the undeformed free surface of the crystal. Thus, the nominal hardness is governed by the geometry of the indenter tip and does not account for surface roughening or sink-in or pile-up of the material. When pile-up does not occur, which is the case in all calculations here, a_N is greater than a. Then, the nominal hardness $H_N := F/a_N$ underestimates the true hardness H.

Nix and Gao [1] have used an argument based on geometrically necessary dislocations to derive a scaling law, which phrased in terms of nominal hardness is

$$\frac{H_N}{H_0} = \sqrt{1 + \frac{h^*}{h}}, \tag{4}$$

for conical indenters. Following a similar approach, Swadener et al [2] developed the expression

$$\frac{H_N}{H_0} = \sqrt{1 + \frac{R^*}{R}}, \tag{5}$$

for spherical indentation. Repeating the developments of [1, 2] but in two dimensions, we find that the expressions (4) and (5) also hold for wedge and circular indenters, respectively.

Figure 9 shows that these expressions give an excellent fit to our data when expressed in terms of nominal hardness. Each of the three curves in this figure are separate fits (with a correlation coefficient that is 0.976 or better), but it is interesting to note that the values of H_0 are between 140 and 177 MPa. The length parameters h^* and R^* are not material length parameters as they depend sensitively on the indenter shape: $h^* = 1.2\,\mu$m for the 70° indenter and is 10 times smaller when $\alpha = 85°$, while $R^* = 6.6\,\mu$m.

The quality of the fit in figure 9 is quite remarkable when considering the assumptions underlying equations (4) and (5). One key assumption in [1, 2] is that the plastic zone has a semi-circular shape (in 2D) with a radius equal to a_N. However, according to figure 4, the plastic zone according to our simulations is much larger and is not semi-circular. Secondly, the square-root scaling originates directly from assuming Taylor hardening, which 2D discrete dislocation plasticity with the constitutive rules used here does not reproduce.

A main reason for the usefulness of indentation hardness measurements is the connection between hardness and strength. For non-hardening isotropic materials one can extract the yield strength from the hardness using the Tabor relation $H \approx 3\sigma_f$. The values of hardness obtained here using circular indenters with R up to $4\,\mu$m correspond to yield strengths that
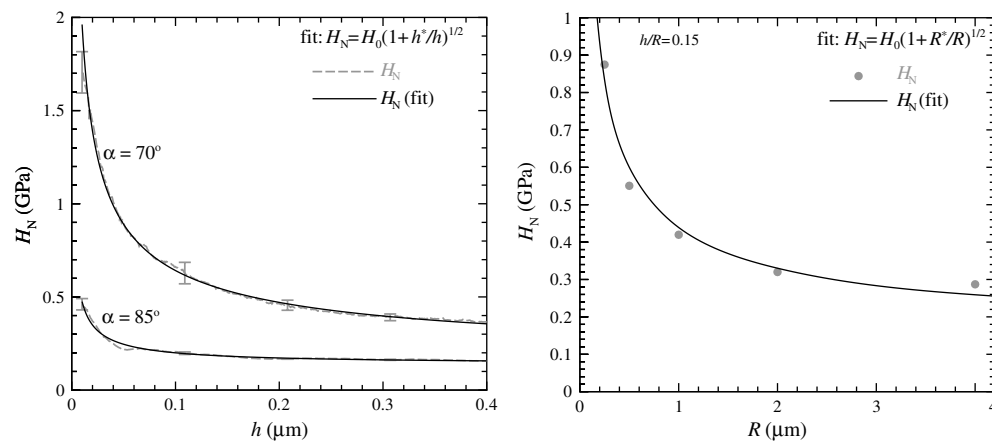
Figure 9. Size dependence of nominal hardness H_N from discrete dislocation computations (blue) and the fits of the scaling laws (4) and (5) for (*a*) wedge and (*b*) circular indenters, respectively.

exceed the uniaxial compression yield strength of approximately 50 MPa by at least a factor of 4. Indeed, Swadener *et al* [2] found that spherical indenters with a radius of a few hundred micrometres were needed before the hardness was no longer size dependent. Wedge indentation approaches the uniaxial yield strength at smaller indentation depths when the tip angle is large ($\alpha = 85°$).

For a wedge indenter with $\alpha = 70°$ and for circular indenters with radii between 0.25 and 4 μm, the force necessary for any indentation depth is only mildly dependent on the tip shape or radius. On the other hand, the hardness as a function of depth is found to be quite sensitive to shape. This shape sensitivity is caused primarily by the contact area evolving in significantly different ways depending on the shape of the indenter.

Acknowledgments

References

[1] Nix W D and Gao H 1998 *J. Mech. Phys. Solids* **43** 411–23
[2] Swadener J G, George E P and Pharr G M 2002 *J. Mech. Phys. Solids* **50** 681–94
[3] Lou J, Shrotriya P, Buchheit T, Yang D and Soboyejo W O 2003 *J. Mater. Res.* **18** 719–28
[4] Mirshams R A and Pothapragada R M 2006 *Acta Mater.* **54** 1123–34
[5] Qu S, Huang Y, Pharr G M and Hwang K C 2006 *Int. J. Plast.* **22** 1265–86
[6] Widjaja A, Van der Giessen E and Needleman A 2005 *Mater. Sci. Eng.* A **400–401** 456–9
[7] Van der Giessen E and Needleman A 1995 *Modelling Simul. Mater. Sci. Eng.* **3** 689–735
[8] Deshpande V S, Needleman A and Van der Giessen E 2003 *Acta Mater.* **51** 1–15
[9] Deshpande V S, Needleman A and Van der Giessen E 2003 *Acta Mater.* **51** 4637–51
[10] Nicola L, Van der Giessen E and Needleman A 2003 *J. Appl. Phys.* **93** 5920–8
[11] Deshpande V S, Needleman A and Van der Giessen E 2005 *J. Mech. Phys. Solids* **53** 2661–91

[12] Nicola L, Xiang Y, Vlassak J J, Van der Giessen E and Needleman A 2006 *J. Mech. Phys. Solids* **54** 2089–110

[13] Widjaja A, Needleman A, Deshpande V S and Van der Giessen E 2006 On contact and size effects in discrete dislocation modelling of wedge indentation submitted

[14] Oliver W C and Pharr G M 1992 *J. Mater. Res.* **7** 1564–83

[15] Johnson K L 1987 *Contact Mechanics* (Cambridge, UK : Cambridge University Press)

[16] Johnson K L 1970 *J. Mech. Phys. Solids* **18** 115–26

[17] Ma Q and Clarke D R 1995 *J. Mater. Res.* **10** 853–63